Supplementary Information

Hydrangea-like Architectures Composed of Zr-based Metal-Organic Framework Nanosheets with Enhanced Iodine Capture

Xiangxiang Wang, [a] Hao Zhang, [a] Chao Qi, [a] Fan Zhou, [a] Linhan Ni, [a] Saisai Chen,[a] Junwen Qi, [a] Chaohai Wang,[a] Tao Zheng, [b,*] and Jiansheng Li [a,*]

a. School of Environmental and Biological Engineering Nanjing University of Science and Technology, Nanjing 210094

b. Yangtze River Delta Research Institute, Northwestern Polytechnical University, Suzhou 215400.

Section S1. Materials and Methods

Materials and Characterization.

Zirconium tetrachloride ($ZrCl_4$, Sigma-Aldrich, ≥98%) and 4',4''',4''''-nitrilotris ([1,1'-biphenyl]-4-carboxylicacid)) (H_3TBPA, 98%) were purchased from Beijing HWRK Chem co. Ltd. N, N-dimethylformamide (DMF), formic acid (88%) and absolute methanol and ethanol were purchased from Shanghai Chemical Reagent Inc of the Chinese Medicine Group. All reagents and solvents were obtained from commercial resources and used without further purification.

Powder X-ray diffraction (PXRD) patterns were collected from 3° to 50°, with a step of 0.02°, and the data collection time was 0.1 s, using a Bruker D8 advance X-ray diffractometer with Cu Kα radiation (λ = 1.54056 Å) equipped with a Lynxeye 1D detector. Single crystal X-ray diffraction (SC-XRD) was performed using a Bruker D8-Venture single crystal X-ray diffractometer equipped with a digital camera. The diffraction data was collected using a Turbo X-ray Source (Mo Kα radiation, = 0.71073 Å) adopting the direct-drive rotating anode technique and a CMOS detector under a temperature of 296 K. Data frames were collected by the program APEX3 and processed using the SAINT routine. Integration of data and multi-scan absorption correction were applied using the program embedded within AEPX3. The structures were solved by the direct method and refined on F2 by full-matrix least-squares methods using SHELXTL-2014[1]. Thermogravimetric analysis (TGA) was performed on a NETZSCH STA 449F3 instrument in the range of 30-900 °C under a nitrogen flow with a heating rate of 10 °C/min for the samples of compounds. A Quantachrome Autosorb Gas Sorption analyzer was used to perform gas adsorption measurements. The FTIR spectrum over a range 4000-400 cm^{-1} were collected on a Thermo Nicolet 6700 instrument. Scanning electron microscopy (SEM) analysis was performed on a JEOL 7800 system. High-resolution TEM was performed on a Tecnai G2 F30 S-TWIN system. Raman spectra of samples before and after iodine adsorption were collected on a Horiba XploRA Raman spectrometer with an excitation line of 532 nm at 10% laser power. The X-ray Photoelectron Spectroscopy (XPS) data of iodine adsorbed samples were conducted on a photoelectron spectrometer (PHI

Quantera II) with Al Kα (1486.6 eV) as the X-ray source. The Atomic Force Microscopy (AFM) images were carried out using a Bruker Multimode 8 scanning probe microscope.

Section S2. Synthesis of compounds

Synthesis of ZrTBPA. H_3TBPA (40 mg, 0.0165 mmol) and $ZrCl_4$ (100 mg, 0.43 mmol) were dissolved in 6 mL of N, N-dimethylformamide (DMF), 4 mL formic acid and 400 μl H_2O, then mixture was placed in a 50 mL Teflon-lined stainless steel vessel and kept at 130 ^oC for 24 hours and then cooled to room temperature, Yellow hexagonal bulky crystals were collected and washing with different solvents DMF (3×50 ml), deionized water (3×50 ml) and ethanol (3×50 ml), successively. After filtering, the resulted powder was dried under vacuum for 24 hours at 80 ^oC.

Synthesis of ZrTBPA-tb. H_3TBPA (40 mg, 0.0165 mmol) and $ZrCl_4$ (100 mg, 0.43 mmol) were dissolved in 7 mL of N, N-dimethylformamide (DMF), 3 mL formic acid and 400 μl H_2O, then mixture was placed in a 50 mL Teflon-lined stainless steel vessel and kept at 130 ^oC for 24 hours and then cooled to room temperature, Yellow hexagonal thin block crystals were collected and washing with different solvents DMF (3×50 ml), deionized water (3×50 ml) and ethanol (3×50 ml), successively. After filtering, the resulted powder was dried under vacuum for 24 hours at 80 ^oC.

Synthesis of ZrTBPA-ns. H_3TBPA (40 mg, 0.0165 mmol) and $ZrCl_4$ (100 mg, 0.43 mmol) were dissolved in 8 mL of N, N-dimethylformamide (DMF), 2 mL formic acid and 400 μl H_2O, then mixture was placed in a 50 mL Teflon-lined stainless steel vessel and kept at 130 ^oC for 24 hours and then cooled to room temperature, yellow precipitation was collected and washing with different solvents DMF (3×50 ml), deionized water (3×50 ml) and ethanol (3×50 ml), successively. After filtering, the resulted powder was dried under vacuum for 24 hours at 80 ^oC.

Section S3. X-ray crystallography data

Table S1. Crystallographic data and structure refinement results for ZrTBPA.

Formula	$C_{83}H_{81}N_2O_{44}Zr_6$
Formula Mass	2357.81
Crystal system	tetragonal
Space group	*I42m*
a (Å)	30.976(7)
b (Å)	30.976(7)
c (Å)	24.946(5)
α	90
β (°)	90
γ	90
V (Å^3)	23936(12)
Z	8
T (K)	296
λ (Å)	0.71073
D (g cm^{-3})	1.309
μ (mm^{-1})	0.578
F(000)	9480
GOF on F^2	1.065
R_1 [a], wR_2 [all data][b]	0. 0388, 0.0749
R_1 [a], wR_2 [$I>2\sigma(I)$][b]	0. 0318, 0.0721
CCDC No.	2071742

[a]$R_1 = \Sigma(F_o - F_c)/\Sigma F_o$; [b]$wR_2 = [\Sigma w(F - F_c)^2/\Sigma w(F_o)^2]^{1/2}$

Table S2: Selected bond lengths (Å) for ZrTBPA.

Selected Bond Lengths (Å)			
Zr1-O9	2.037(7)	Zr2-O5	2.252(8)
Zr1-O10	2.059(5)	Zr3-O9	2.078(7)
Zr1-O6	2.221(8)	Zr3-O4	2.188 (8)
Zr1-O1	2.194(7)	Zr3-O18	2.274 (9)
Zr1-O11	2.223(8)	Zr3-O15	2.295 (11)
Zr1-O16	2.270(7)	Zr3-O16	2.316 (10)
Zr1-O17	2.226(9)	Zr4-O9	2.063 (7)
Zr1-O8	2.374(7)	Zr4-O7	2.089 (6)
Zr2-O7	2.106(10)	Zr4-O12	2.217 (8)
Zr2-O14	2.187(9)	Zr4-O3	2.253 (8)
Zr2-O10	2.079(10)	Zr4-O8	2.241 (7)
Zr2-O8	2.246(7)	Zr4-O15	2.263 (6)
Zr2-O7	2.106(10)	Zr4-O2	2.278 (8)

Table S3. Bond valence sum (BVS) analysis[2] for bridging O of ZrTBPA

Atoms	O_7	O_8	O_9	O_{10}	O_{15}	O_{16}
BVS	1.90	1.16	2.11	2.05	1.21	1.13

Bridging O entities are O^{2-}, OH^-. For Zr_6 clusters, there are eight μ_3-O atoms, O_7, O_8(symmetry), O_9(symmetry), O_{10}, O_{15} and O_{16}, it is found by Bond valence sum (BVS) calculation, O_7, O_9, O_{10} are μ_3-O^{2-}, while O_8, O_{15} and O_{16} are μ_3-OH^{-1}.

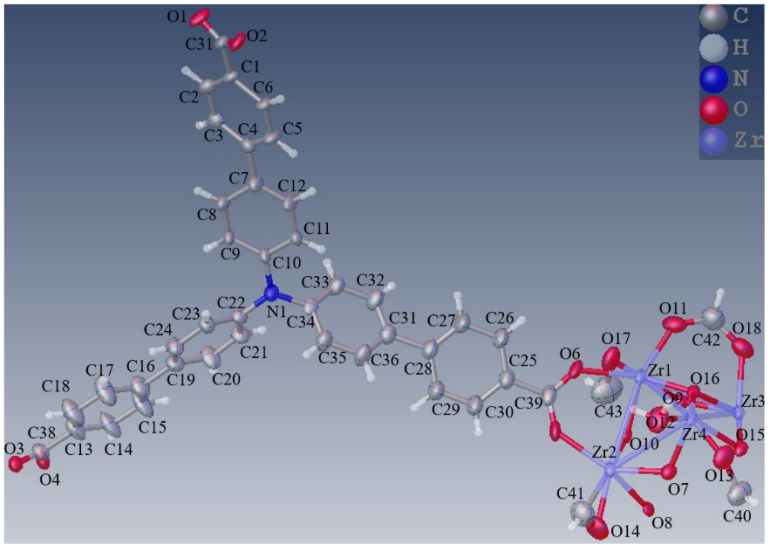

Fig. S1 The asymmetric unit of ZrTBPA with thermal ellipsoids model.

Section S4. The control process of crystals

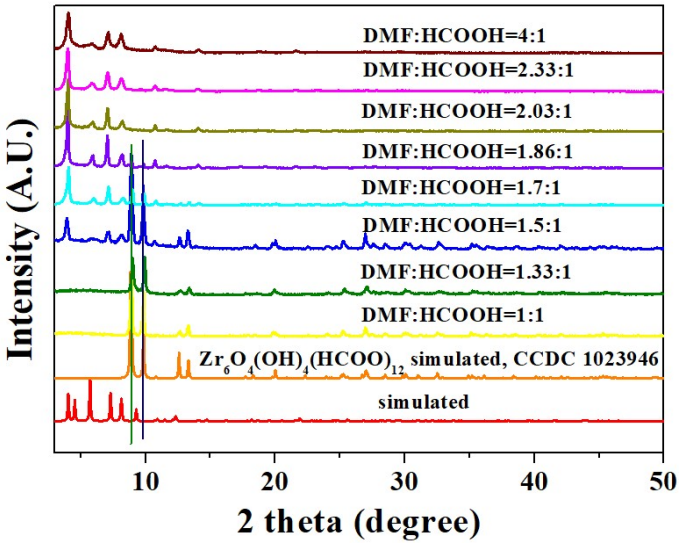

Fig. S2. The PXRD patterns of regulatory Zr-MOFs by changing the volume ratios of DMF to formic acid.

The high-quality crystals were obtained through the solvothermal reaction of $ZrCl_4$ and H_3TBPA in a mixture of DMF and formic acid (HCOOH) modulator, water with the volume ratio of 15:10:1 at 130 °C for 24 h under autogenous pressure. However, they have notable crystalline impurities, the other phase was zirconium formate with the formula of $[Zr_6O_4(OH)_4(FA)_{12}]\cdot DMF\cdot 6H_2O$ (FA= formic acid). Single-phase zirconium formate was formed when the volume ratios of DMF and formic acid were in the range of 1-1.5. When the ratios were between 1.5 and 2, two-phase including Zr-MOFs and zirconium formate were

formed. The pure phase of Zr-MOFs were achieved when the ratios are in the 2-4 range (Fig. S 3a). What's really interesting is that the generated crystals become thinner and thinner with the increasing volume ratios of DMF to HCOOH. The morphology changes from the previous hexagon block to final hydrangeas-shape nanosheet (Fig. S3b).

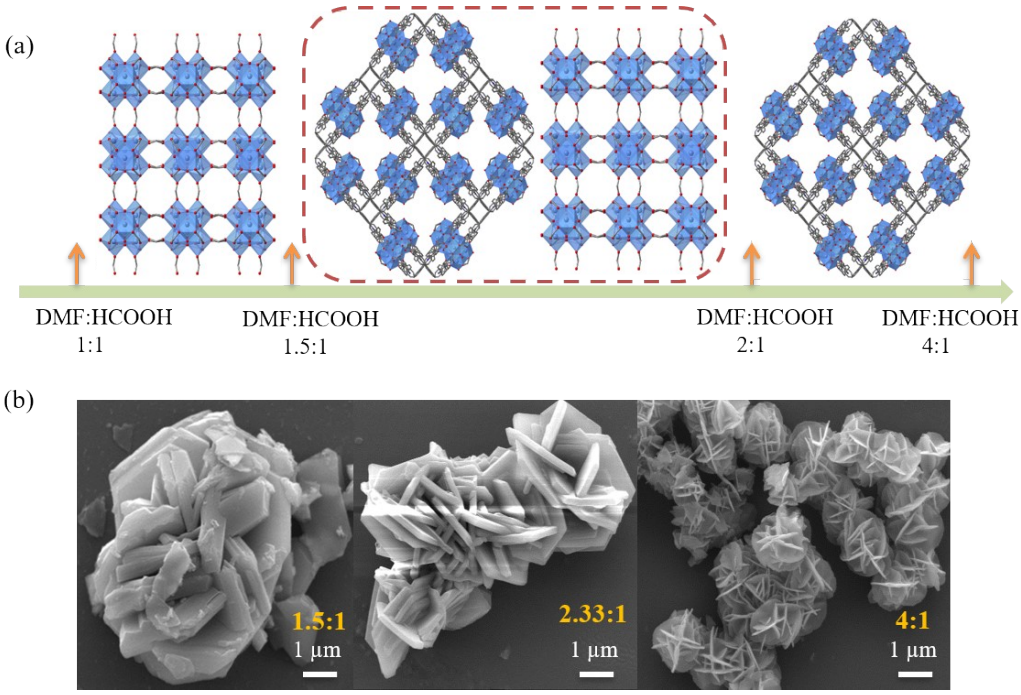

Fig. S3. (a) Phase diagram in the range of different volume ratios of DMF to formic acid. (b) Morphological evolution of various volume ratios of DMF to formic acid.

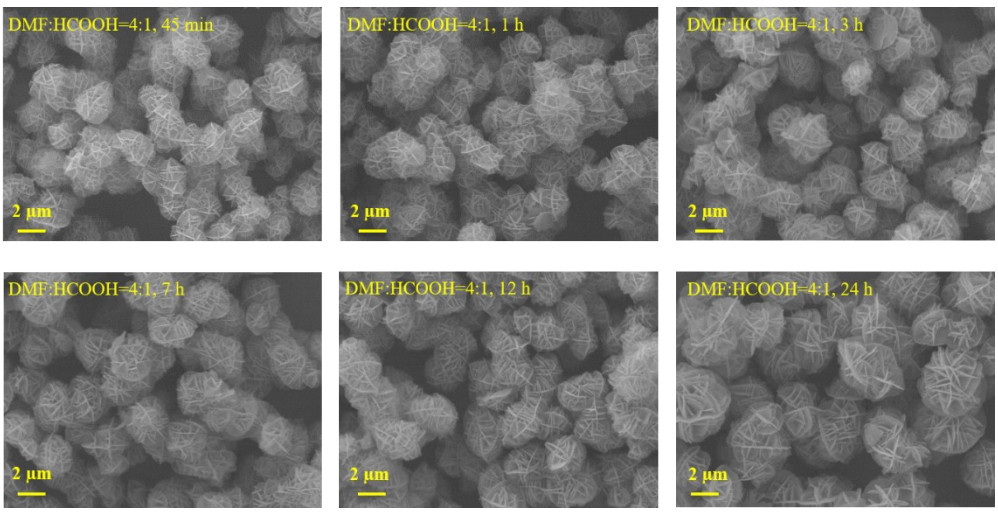

Fig. S4. SEM images of the time dependent experiments of ZrTBPA-ns.

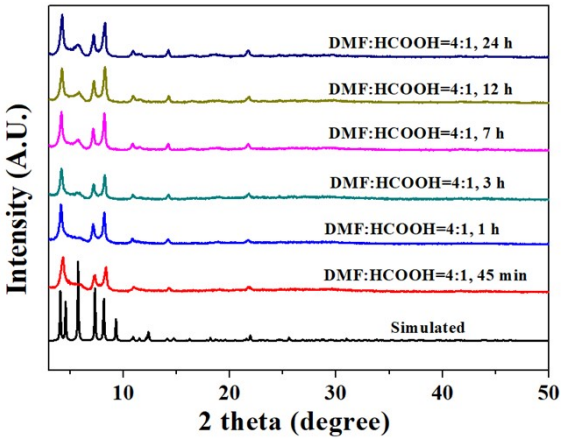

Fig. S5. PXRD patterns of the time dependent experiments of ZrTBPA-ns.

Section S5. Surface area measurements

Volumetric gas adsorption measurements for ZrTBPA-tb and ZrTBPA-ns were measured at 77 K with a liquid nitrogen bath, the detecting pressures range from 0 to 760 Torr respectively. All the measurements were conducted in the presence of high-purity gases. Soaking them in methanol solution for 48 h to exchange high boiling point and large volume DMF molecules in the pore. Meanwhile, fresh methanol was added every 6 h, after filtering, the resulted powders were dried under vacuum for 24 hours at 60 °C. After decanting the methanol extract, the sample was dried under a dynamic vacuum (<10^{-3} Torr) at room temperature overnight. Before adsorption measurement, the sample was activated using the "outgas" function of the surface area analyzer for 12 h at 120 °C.

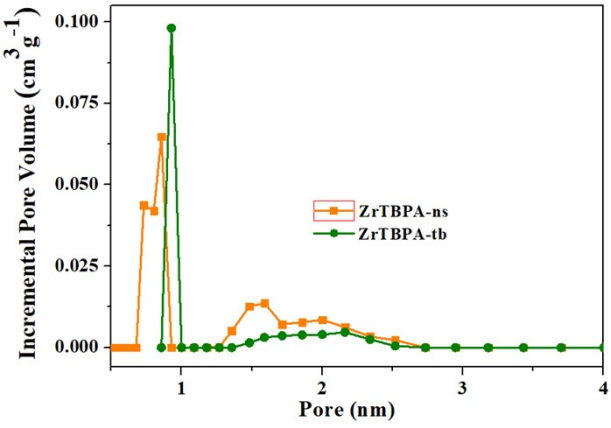

Fig. S6. Pore size distribution of ZrTBPA-tb and ZrTBPA-ns calculated using nonlocal density function theory (NLDFT).

Table S4 Physical properties of the samples

Samples	Morphology	Crystal size (μm)	Thickness (nm)	Pore volume (cm^3/g)	S_{BET} (m^2/g)
ZrTBPA-tb	Hexagonal thin block	8	450	0.17	349.6
ZrTBPA-ns	hydrangeas-like nanosheets	4	43	0.28	551.9

Section S6. Stability Measurements

pH Stability Measurements. Hydrolytic stability measurements for ZrTBPA-tb and ZrTBPA-ns were studied by soaking the samples into HNO_3 (1 M, 2 M, 4 M and 6 M) and NaOH (pH = 10, 12) solutions at room temperature for 24 h.

Solvents Stability Measurements. Solvents resistance measurements for ZrTBPA-tb and ZrTBPA-ns were studied by soaking the samples into a variety of solvents including, DMF, cyclohexane, methanol, acetonitrile and water at room temperature for 24 h.

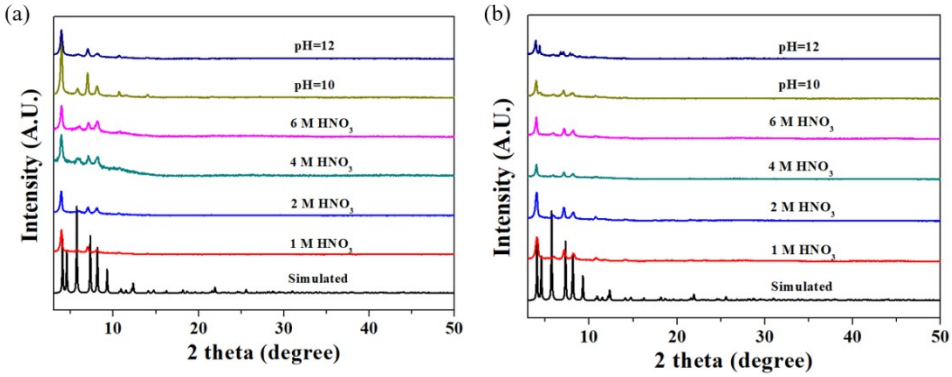

Fig. S7. The PXRD patterns for ZrTBPA-tb (a) and ZrTBPA-ns (b) after immersed in aqueous solutions at different pH values.

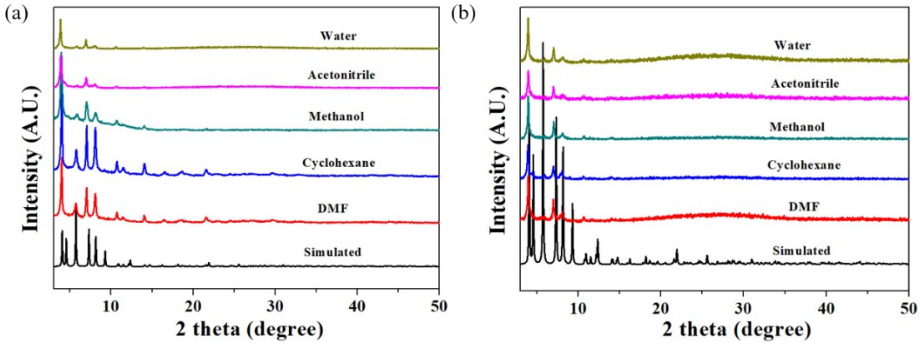

Fig. S8. The PXRD patterns for ZrTBPA-tb (a) and ZrTBPA-ns (b) after immersed in various solvents.

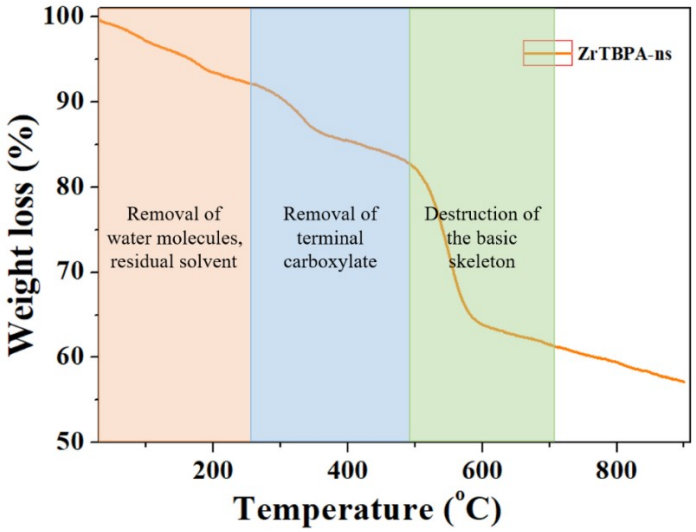

Fig. S9. TG curve of ZrTBPA-ns

The thermostability of nanosheets ZrTBPA-ns is measured by thermogravimetric analysis (TGA). Weight losses of ZrTBPA-ns can be divided into three distinct stages. The first stage from 30 to 260 °C corresponds to the loss of volatilization of physically adsorbed water, residual solvent in the void space and coordinated water molecules. In the second stage (260-495 °C), the weight loss corresponds to the terminal carboxylate. The third stage (>495 °C) suggests the destruction of the basic skeleton of ZrTBPA-ns.

Section S7. Iodine Vapor Adsorption and Release

Pretreatment of samples. Soaking ZrTBPA-tb and ZrTBPA-ns in methanol solution for 48 h to exchange high boiling point and large volume DMF molecules in the pore. Meanwhile, fresh methanol was added every 6 h. After filtering, the final powders were dried under vacuum for 24 hours at 80 °C.

Iodine Vapor Adsorption Measurement. Two independent open sample vials containing 15 mg samples and 300 mg iodine solid were placed in a 100 ml sealed bottle and kept at 75 °C for iodine capture. After the reaction, opening the bottle and cooling to the room temperature, the vial containing the iodine adsorbed sample was weighed periodically until the mass of it remained unchanged. The iodine adsorption capacity, Q (g/g), was measured by the weighing method and calculated using $Q = (w_2-w_1)/w_1$, where w_1 and w_2 are the masses of adsorbed samples before and after iodine adsorption, respectively.

Iodine Release. The iodine-loaded samples were soaked in fresh ethanol at room temperature, Keep changing the fresh ethanol solution until the solution solution becoming clear.

Study on adsorption process

The Weber-Morris intraparticle mass transfer diffusion model was adopted to study the adsorption process. The mathematical equation of these kinetic model is represented as follows[3]:

Weber and Morris (W-M) model: $q_t = k_d t^{0.5} + C$

where k_d (mg/g/min$^{0.5}$) represents the diffusion rate constant within the adsorbent; and C is a constant related to the thickness of the boundary layer.

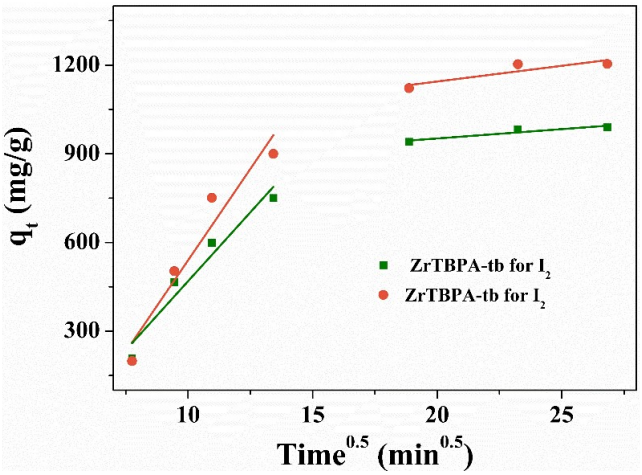

Fig. S10. The intraparticle diffusion model for iodine adsorption.

Table S5 Intraparticle diffusion model parameters for the adsorption of iodine on ZrTBPA-tb and ZrTBPA-ns.

Samples	First phase			Second phase		
	K_{d1}(mg·g^{-1}·min$^{0.5}$)	C_1	R^2	K_{d2}(mg·g^{-1}·min$^{0.5}$)	C_2	R^2
ZrTBPA-tb	93.24	-463.16	0.95	6.31	825.95	0.89
ZrTBPA-ns	123.58	-695.91	0.94	10.60	932.84	0.81

The corresponding results show that the fitting linear curves don't go through the origin (Fig.S10). The multilinearity with two different stages demonstrates that the process involves a multi-stage process. The first rapid process presents the transfer of iodine from gas phase to the adsorbent's surface. The second gradually diffused process infers the intraparticle diffusion of iodine from the surface to the adsorbent's sites. From Table S5, the diffusion rate constants of ZrTBPA-ns in both two adsorption stages are 123.58 mg·g^{-1} min$^{0.5}$and 10.60 mg·g^{-1} min$^{0.5}$, which are 32.5% and 68.0% higher than that of ZrTBPA-tb, respectively. This

enhanced diffusion process on ZrTBPA-ns could be attributed to the lower mass transfer resistance of iodine in nanosheet.

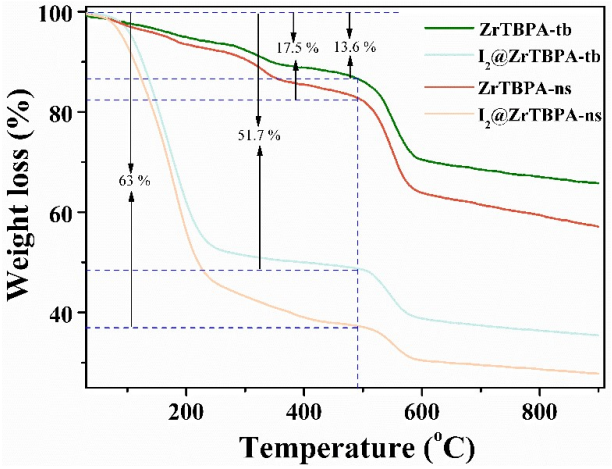

Fig. S11. TGA curves of bare and iodine vapor adsorbed ZrTBPA-tb and ZrTBPA-ns.

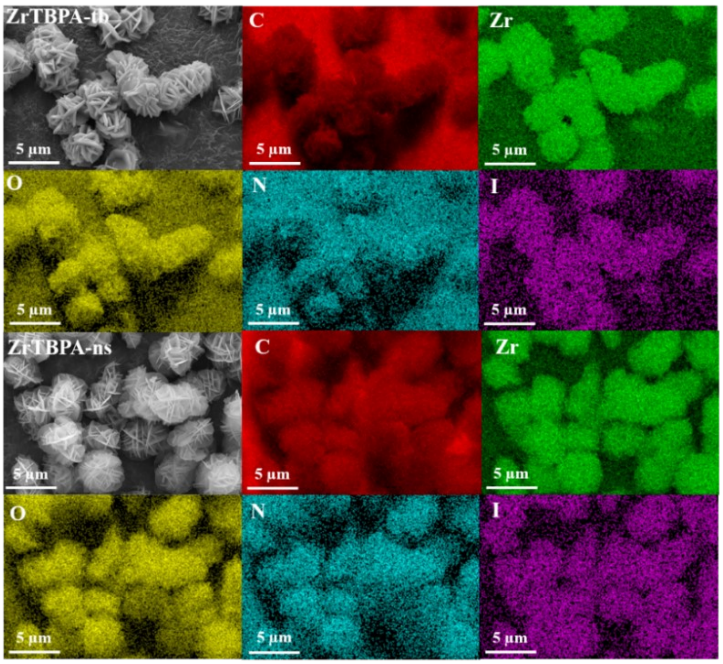

Fig. S12. SEM-EDS mapping of ZrTBPA-tb and ZrTBPA-ns after absorption of I_2 vapor.

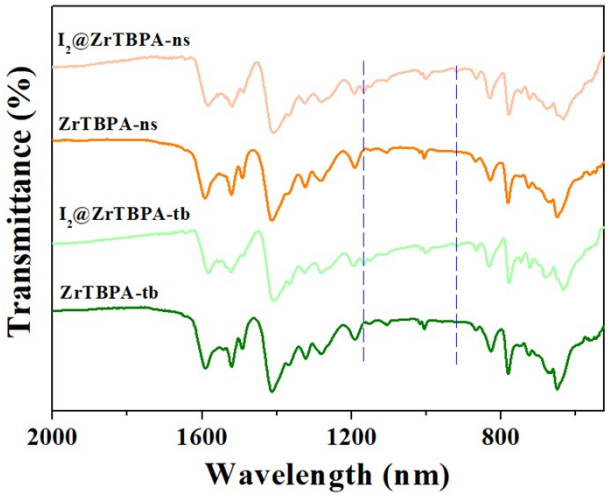

Fig. S13. FTIR spectrum of bare and iodine vapor adsorbed ZrTBPA-tb and ZrTBPA-ns.

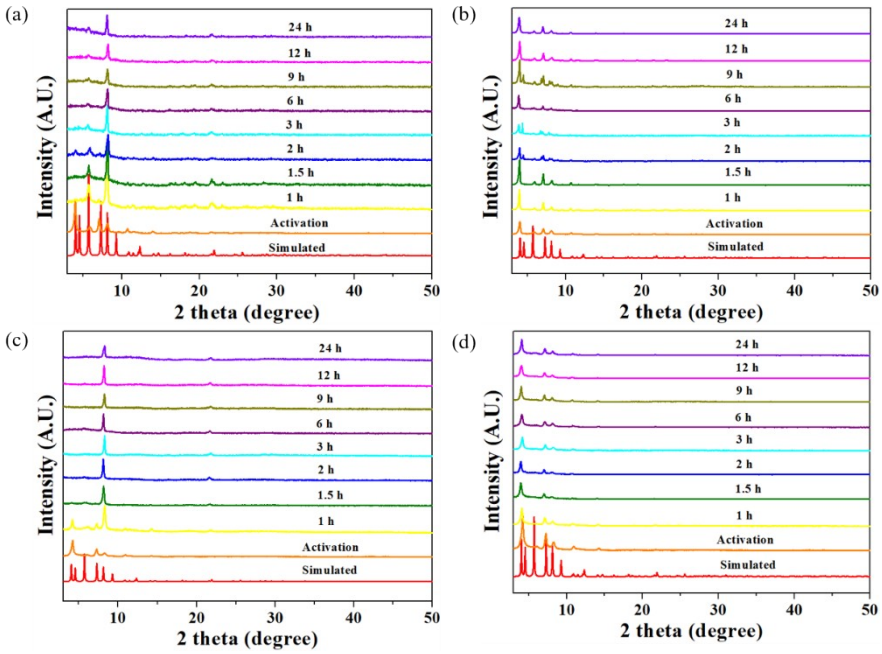

Fig. S14. PXRD patterns of ZrTBPA-tb and ZrTBPA-ns with different iodine loading time, respectively (a, c). PXRD patterns of ZrTBPA-tb and ZrTBPA-ns with different iodine loading time eluted by ethanol, respectively (b, d).

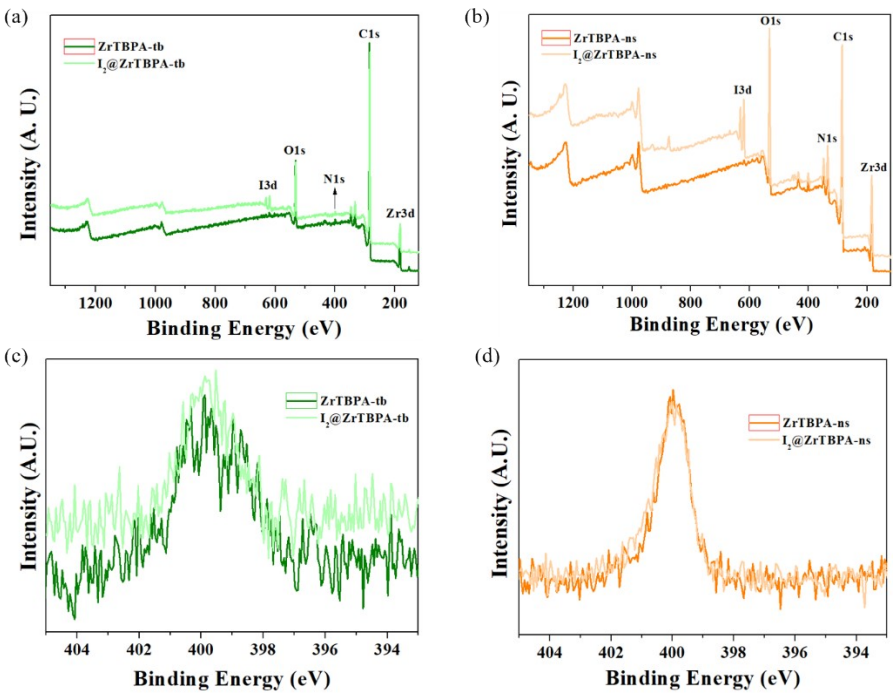

Fig. S15. Wide-scan XPS spectra of pristine and iodine-loaded ZrTBPA-tb (a) and ZrTBPA-ns (b)N1s XPS spectra of ZrTBPA-tb (a) and ZrTBPA-ns (b) before and after iodine vapor adsorption.

Table S6: Iodine vapor adsorption capacities of different MOF-based adsorbents.

MOFs adsorbents	Surface area ($m^2\ g^{-1}$)	I_2 sorption capacity ($g\ g^{-1}$)	Temperature (^oC)	Refs.
UPC-158	2170	1.78	70	Ref [4]
$Zr_6O_4(OH)_4(peb)_6$	1328	2.79	RT	Ref [5]
$Zr_6O_4(OH)_4(bdb)_6$	3850	1.85	RT	Ref [5]
$Zr_6O_4(OH)_4(edb)_6$	3300	1.85	RT	Ref [5]
Co_2(m-DOBDC)	1328	2.02	75	Ref [6]
MIL-53-$(SH)_2$	324	0.33	RT	Ref [7]
MOF-808	1930	2.18	80	Ref [8]
NU-1000	2126	1.45	80	Ref [8]
MOF-867	2638	0.88	80	Ref [8]
UiO-66	1072	0.66	80	Ref [8]
UiO-67	2638	0.53	80	Ref [8]
HKUST-1	1850	1.75	75	Ref [9]
ZIF-8	1837	1.25	77	Ref [10]
MFM-300 (Fe)	1192	1.29	70	Ref [11]
MFM-300 (In)	1050	1.16	70	Ref [11]
MFM-300 (Al)	1370	0.94	70	Ref [11]
$Zr_6O_4(OH)_4(sdc^*)_6$	2900	1.07	RT	Ref [5]
SBMOF-1	145.2	0.23	RT	Ref [12]
SBMOF-2	195	0.43	RT	Ref [12]
$Ni^{II}(pz)Ni^{II}(CN)_4$	-	0.59	80	Ref [13]
Cu-BTC@PES	237.42	0.64	75	Ref [14]
Cu_2O/TMU-17-NH_2	-	0.30	60	Ref [15]
JNU-200	466.5	1.08	80	Ref [16]
UiO-66-NH-B.D	406.3	1.17	75	Ref [17]
Th-SINAP-8	650.4	0.47	80	Ref [18]

Th-UiO-66-$(NH_2)_2$	628.8	0.97	80	Ref [19]
Th-SINAP-9	265.2	0.81	80	Ref [20]
NUC-5	1594	0.78	77	Ref [21]
AlOC-27-NC	-	0.53	80	Ref [22]
SION-8	509	0.25	75	Ref [23]
ZrTBPA-tb	551.9	0.95	75	This work
ZrTBPA-ns	349.6	1.20	75	This work

References

1. G. M. Sheldrick, *Acta Crystallogr. C.*, 2015, **71**, 3-8.
2. N. Brese and M. O'keeffe, *Acta Crystallogr. B.*, 1991, **47**, 192-197.
3. W. J. Weber Jr and J. C. Morris, *J. Saint. Eng. Div.,* 1963, **89**, 31-59.
4. B. Guo, F. Li, C. Wang, L. Zhang and D. Sun, *J. Mater. Chem. A*, 2019, **7**, 13173-13179.
5. R. J. Marshall, S. L. Griffin, C. Wilson and R. S. Forgan, *Chemistry*, 2016, **22**, 4870-4877.
6. B. Lee, Y. P. Chen, J. Park and J. Park, *ACS Appl. Mater. Interfaces*, 2019, **11**, 25817-25823.
7. A. S. Munn, F. Millange, M. Frigoli, N. Guillou, C. Falaise, V. Stevenson, C. Volkringer, T. Loiseau, G. Cibin and R. I. Walton, *CrystEngComm.*, 2016, **18**, 8108-8114.
8. P. Chen, X. He, M. Pang, X. Dong, S. Zhao and W. Zhang, *ACS Appl. Mater. Interfaces*, 2020, **12**, 20429-20439.
9. D. F. Sava, K. W. Chapman, M. A. Rodriguez, J. A. Greathouse, P. S. Crozier, H. Zhao, P. J. Chupas and T. M. Nenoff, *Chem.Mater.*, 2013, **25**, 2591-2596.
10. D. F. Sava, M. A. Rodriguez, K. W. Chapman, P. J. Chupas, J. A. Greathouse, P. S. Crozier and T. M. Nenoff, *J. Am. Chem. Soc.*, 2011, **133**, 12398-12401.
11. X. Zhang, I. da Silva, H. G. W. Godfrey, S. K. Callear, S. A. Sapchenko, Y. Cheng, I. Vitorica-Yrezabal, M. D. Frogley, G. Cinque, C. C. Tang, C. Giacobbe, C. Dejoie, S. Rudic, A. J. Ramirez-Cuesta, M. A. Denecke, S. Yang and M. Schroder, *J. Am. Chem. Soc.*, 2017, **139**, 16289-16296.
12. D. Banerjee, X. Chen, S. S. Lobanov, A. M. Plonka, X. Chan, J. A. Daly, T. Kim, P. K. Thallapally and J. B. Parise, *ACS Appl. Mater. Interfaces*, 2018, **10**, 10622-10626.
13. G. Massasso, J. Long, J. Haines, S. Devautour-Vinot, G. Maurin, A. Grandjean, B. Onida, B. Donnadieu, J. Larionova, C. Guerin and Y. Guari, *Inorg. Chem.*, 2014, **53**, 4269-4271.
14. Q. Zhao, L. Zhu, G. Lin, G. Chen, B. Liu, L. Zhang, T. Duan and J. Lei, *ACS Appl. Mater. Interfaces*, 2019, **11**, 42635-42645.
15. M. Yadollahi, H. Hamadi and V. Nobakht, *J. Hazard. Mater*, 2020, **399**, 122872.
16. K. Wu, Y.-L. Huang, J. Zheng, D. Luo, M. Xie, Y. Y. Li, W. Lu and D. Li, *Mater. Chem. Fron.*, 2021, DOI: 10.1039/d1qm00211b.
17. M. Zahid, D. Zhang, X. Xu, M. Pan, M. H. ul haq, A. T. Reda and W. Xu, *J. Hazard. Mater.*, 2021, **416**, 125835.
18. Z. J. Li, Z. Yue, Y. Ju, X. Wu, Y. Ren, S. Wang, Y. Li, Z. H. Zhang, X. Guo, J. Lin and J. Q. Wang, *Inorg. Chem.*, 2020, **59**, 4435-4442.

19.Z. J. Li, Y. Ju, H. Lu, X. Wu, X. Yu, Y. Li, X. Wu, Z. H. Zhang, J. Lin, Y. Qian, M. Y. He and J. Q. Wang, *Chemistry*, 2021, **27**, 1286-1291.
20.Z. J. Li, Y. Ju, B. Yu, X. Wu, H. Lu, Y. Li, J. Zhou, X. Guo, Z. H. Zhang, J. Lin, J. Q. Wang and S. Wang, *Chem. Commun.*, 2020, **56**, 6715-6718.
21.H. Chen, L. Fan, X. Zhang and L. Ma, *ACS Appl. Mater. Interfaces*, 2020, **12**, 27803-27811.
22.S. Yao, W. H. Fang, Y. Sun, S. T. Wang and J. Zhang, *J. Am. Chem .Soc.*, 2021, **143**, 2325-2330.
23.A. Gladysiak, T. N. Nguyen, M. Spodaryk, J. H. Lee, J. B. Neaton, A. Zuttel and K. C. Stylianou, *Chemistry*, 2019, **25**, 501-506.